28. See the supplementary materials on *Science* Online.
29. C. Bi, Y. Yuan, Y. Fang, J. Huang, *Adv. Energy Mater.* 10.1002/aenm.201401616 (2014).
30. K. Tvingstedt *et al.*, *Sci. Rep.* **4**, 6071 (2014).
31. S. De Wolf *et al.*, *J. Phys. Chem. Lett.* **5**, 1035–1039 (2014).
32. A. Sadhanala *et al.*, *J. Phys. Chem. Lett.* **5**, 2501–2505 (2014).
33. R. L. Milot, G. E. Eperon, H. J. Snaith, M. B. Johnston, L. M. Herz, *Adv. Funct. Mater.* **25**, 6218–6227 (2015).
34. W. Tress *et al.*, *Adv. Energy Mater.* 10.1002/aenm.201400812 (2014).
35. H. J. Snaith, *Adv. Funct. Mater.* **20**, 13–19 (2010).
36. U. Rau, *Phys. Rev. B* **76**, 085303 (2007).
37. L. Mazzarella *et al.*, *Appl. Phys. Lett.* **106**, 023902 (2015).

ACKNOWLEDGMENTS

This project was funded in part by the Engineering and Physical Sciences Research Council through the Supergen Solar Energy Hub SuperSolar (EP/M024881/1, EP/M014797/1) and the European Research Council through the Stg-2011 Hybrid Photovoltaic Energy Relays and the European Union Seventh Framework Programme (FP7/2007-2013) under grant agreement 604032 of the MESO project, and the U.S. Office of Naval Research. M.H. is funded by Oxford PV Ltd. W.R. is supported by the Hans-Boeckler-Foundation. We thank our colleagues from the Centre For Renewable Energy Technologies Photovoltaic Measurement and Testing Laboratory, Loughborough University, for their contributions to the measurements of the semi-transparent devices. We also thank K. Jacob and M. Wittig [Helmholtz-Zentrum Berlin (HZB), Institute for Silicon Photovoltaics], L. Mazzarella, and S. Kirner (HZB, Institute PVcomB) for their contributions to fabricating the SHJ cell. The University of Oxford has filed a patent related to this work. The project was designed and conceptualized by D.M. and H.J.S. D.M. performed experiments, analyzed data, and wrote the first draft of the paper. G.S. fabricated and measured devices with semi-transparent electrodes. W.R. characterized the material using THz spectroscopy. G.E. helped with the experimental work and provided technical feedback on the writing of the paper. M.S. provided input and technical direction on the FA/Cs cation mixture. M.H. performed simulations for the optical modeling and calculated the maximum achievable V_{OC}. A.H. analyzed XRD data. N.S. provided input on the preparation of thin films using chemical bath depositions. L.K. and B.R. designed and supervised the fabrication of the SHJ cells. M.J. performed and analyzed EQE measurements. L.H. supervised and analyzed the THz spectroscopy measurements. H.J.S. supervised the overall conception and design of this project. All authors contributed to the writing of the paper.

SUPPLEMENTARY MATERIALS

www.sciencemag.org/content/351/6269/151/suppl/DC1
Materials and Methods
Supplementary Text
Figs. S1 to S15
References (*38*–*42*)

5 October 2015; accepted 3 December 2015
10.1126/science.aad5845

FOREST ECOLOGY

Dominance of the suppressed: Power-law size structure in tropical forests

C. E. Farrior,[1,2]* S. A. Bohlman,[3,4] S. Hubbell,[4,5] S. W. Pacala[6]

Tropical tree size distributions are remarkably consistent despite differences in the environments that support them. With data analysis and theory, we found a simple and biologically intuitive hypothesis to explain this property, which is the foundation of forest dynamics modeling and carbon storage estimates. After a disturbance, new individuals in the forest gap grow quickly in full sun until they begin to overtop one another. The two-dimensional space-filling of the growing crowns of the tallest individuals relegates a group of losing, slow-growing individuals to the understory. Those left in the understory follow a power-law size distribution, the scaling of which depends on only the crown area–to–diameter allometry exponent: a well-conserved value across tropical forests.

Tree size distributions—the frequency of trees by size—are important emergent properties of forests. Tree size distributions signal community-level interactions, are a critical diagnostic of the accuracy of scaling in mechanistic models, and are the basis of many aboveground forest carbon estimates (*1*–*3*). Despite differences in the tree vital rates that determine them, tropical forests worldwide have tree size distributions that follow tight power functions with very similar scaling for a wide range of diameters and commonly have deviations in the tails (*4*, *5*) (Fig. 1). Such a consistent emergent pattern begs an explanation, one that is likely to provide an important key to understanding the mechanisms governing tropical forest dynamics (*6*).

Current theories explaining the consistency of tropical forest size structure are controversial. Explanations based on scaling up individual metabolic rates (*4*, *7*, *8*) are criticized for ignoring the importance of asymmetric competition for light in causing variation in dynamic rates (*9*–*11*). Other theories, which embrace competition and scale individual tree vital rates through an assumption of demographic equilibrium (*5*, *10*, *12*, *13*), are criticized for lacking parsimony, because predictions rely on site-level, size-specific parameterizations (*14*). Despite their differences, common to these theories is the notion that the predicted size structure is a property of steady-state forests far removed from the influence of disturbance. We tested this prediction. We explored the size structure within a well-studied tropical forest and, with theoretical corroboration, present a parsimonious and biologically intuitive explanation for the power-function size structure, observed deviations, and the consistency of the scaling across forests.

[1]National Institute for Mathematical and Biological Synthesis, Knoxville, TN 37996, USA. [2]Department of Integrative Biology, University of Texas at Austin, Austin, TX 78712, USA. [3]School of Forest Resources and Conservation, University of Florida, Gainesville, FL 32611, USA. [4]Smithsonian Tropical Research Institute, Apartado 0843–03092, Balboa, Ancon, Republic of Panama. [5]Department of Ecology and Evolutionary Biology, University of California, Los Angeles, CA 90095, USA. [6]Department of Ecology and Evolutionary Biology, Princeton University, Princeton, NJ 08544, USA.
***Corresponding author. E-mail: cfarrior@nimbios.org**

We explored temporal and spatial patterns in tropical forest size structure in 50 ha and 30 years of data from Barro Colorado Island, Panama (BCI) (*15*–*17*). Forest patches in the early stages of recovery from small-scale disturbances (*18*) develop a power function that extends through a greater range of diameters as time progresses (Fig. 2). At 25 to 30 years after disturbance, the power function extends through the full range of diameters present, and unlike in younger patches, a power law is a likely model of the data [(*18*), criteria following (*19*)]. However, the power-law fit is again lost in patches with more than 30 years since the last disturbance.

Having reached the limit of our temporal analyses, we examined forest patches as grouped by forest size. We used the metric D^*_{est} as an estimate of the size threshold for tree canopy status in a patch (*18*). For each range of D^*_{est}, we fit a power function (with the same scaling as Fig. 1, fit to all data) that transitions at a single size class to an exponential distribution (Fig. 3A) (*18*). This best-fit size class of transition increases with D^*_{est} (Fig. 3B, $P = 0.005$, t test, R-squared = 0.76,

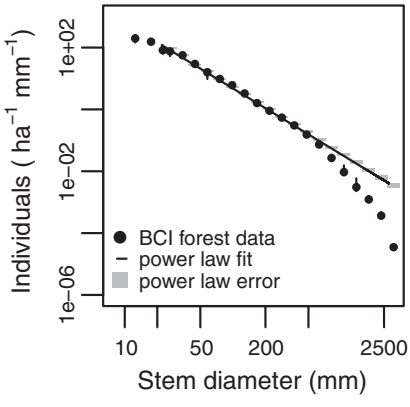

Fig. 1. Size distribution of the 50-ha tropical forest dynamics plot on BCI. The average (points) and range (bars) by size class among all seven censuses are shown. The best-fit power law distribution to all diameters from censuses 3 to 7 (*18*) is drawn (black line). The expected range of variation for that power law, given the average census sample size by size class, is in gray [95% range (*18*)].

N = 6 ranges of D^*_{est} slope = 1.23 mm mm^{-1}). Trees that are likely in the understory, with diameters less than their patch's D^*_{est}, are well characterized by the power function, whereas those that are likely in the canopy are not.

We have three main empirical results: (i) Power-function size structure emerges progressively after likely gap-generating disturbances (Figs. 1 and 2); (ii) understory trees, but not canopy trees, generally follow power-function structure (Fig. 3); and (iii) forest patches far in time from the last local disturbance are responsible for the deviations in the high tail of the landscape-level distribution (Fig. 2). Together these pieces of evidence point to a new hypothesis: Small-scale, gap-generating disturbances maintain power-function size structure whereas later-successional forest patches are responsible for deviations in the high tail. To explore and test this hypothesis, we turned to a model.

In a small, gap-sized patch of forest (1000 m^2), the simulation started from bare ground. Individuals were characterized by their diameter (d) and crown area (ϕd^{θ}). Crown area is the projected two-dimensional area of a tree's canopy. We assumed that the allometric exponent θ was a constant, following theoretical predictions at the individual-plant level (*20*, *21*). Seedlings recruit at a constant rate and grow in diameter in full sun at a constant rate with a constant probability of mortality until the canopy closes. Assuming phototropic growth (*22*), when the sum of the crown areas of all trees exceeds the patch area, the canopy closes. At this point, the largest individuals whose summed crown area is less than the patch size remain in full sun, maintaining canopy growth and mortality rates. All other individuals are overtopped and grow in the understory at a single slower rate and have a single higher probability of mortality. At each time step, the patch has a probability of a gap-generating disturbance, setting the patch back to bare ground. A forest landscape is assembled by compiling snapshots of the simulation (*18*). We estimated all model parameters (table S1) from BCI individual tree vital-rate data (*18*), except for the gap-generating disturbance rate, which was estimated from the central Amazon (*2*) and assumed to be responsible for half of the observed canopy mortality. The critical parameter of θ (1.28) was measured directly on BCI (*22*).

The resulting landscape-level size distribution matches the probability distribution of diameters on BCI well throughout the full range of the diameters (Fig. 4A). It captures the power function throughout intermediate diameters and the departures in both tails. Size-dependent demographic rates also compare well with this simple model (fig. S2). To understand the mechanisms that generate this goodness of fit, we turn to its mathematical approximation.

Consider the succession of a single patch of forest (size P), initiated by one cohort of seedlings after a patch-clearing disturbance. After the canopy closes, the number of canopy individuals (N_c) is a function of only their size (stem diameter d_c and crown area = ϕd_c^{θ})

$$N_c = \frac{P}{\phi d_c^{\theta}} \quad (1)$$

As trees grow, the number that can fit in the canopy decreases

$$\frac{dN_c}{dd_c} = \frac{-P\theta}{\phi d_c^{\theta+1}} \quad (2)$$

The decrease in canopy trees is achieved in two ways: random mortality (μ_c), which kills the trees, and overtopping, which moves canopy trees to the understory. Over the time period it takes for 1 mm of growth in stem diameter (G_c^{-1})

$$\frac{P\theta}{\phi d_c^{\theta+1}} = \text{new understory trees} + \frac{\mu_c}{G_c}\frac{P}{\phi d_c^{\theta}} \quad (3)$$

While d_c is small, new understory trees in Eq. 3 are approximately equal to $\frac{P\theta}{\phi d^{\theta+1}}$, which is a power law in d of scaling –(θ + 1) (Fig. 4B). Taking the approximation that the slow-growing understory trees do not grow at all (G_u = 0) (*23*, *24*) and have

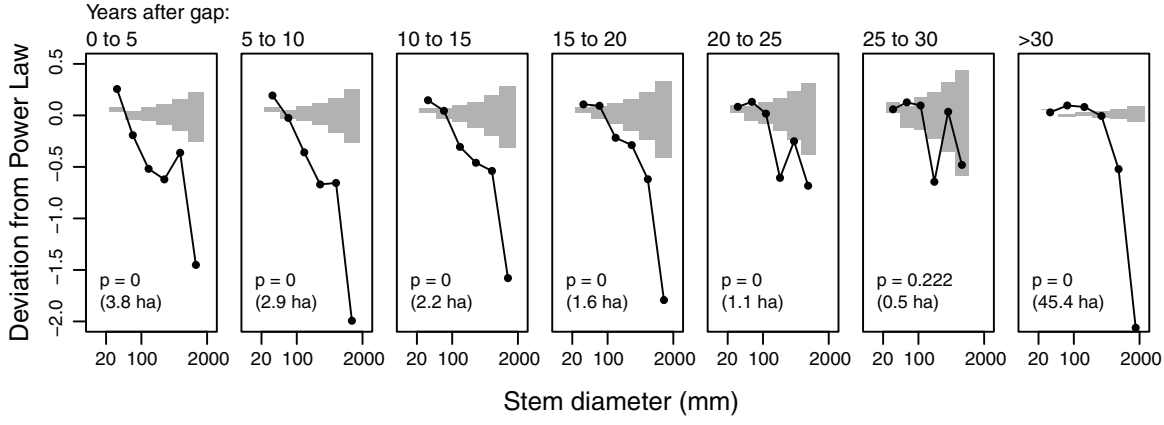

Fig. 2. Tree size distributions and time since local disturbance. Size distributions for combined 5 m by 5 m subplots at the same time in recovery (panel titles) from a gap (*18*). For clarity, deviations in log space from the power law are plotted (black, individuals mm^{-1} ha^{-1}). The area sampled is shown (in ha). Gray shows the expected range of deviation for the power law, given the area of data sampled (95% confidence interval). The P values are the proportion of synthetic distributions that fit worse than the data to the power law, using the Kolmogorov-Smirnov statistic as the metric of goodness of fit [P > 0.1 indicates a likely fit (*18*)].

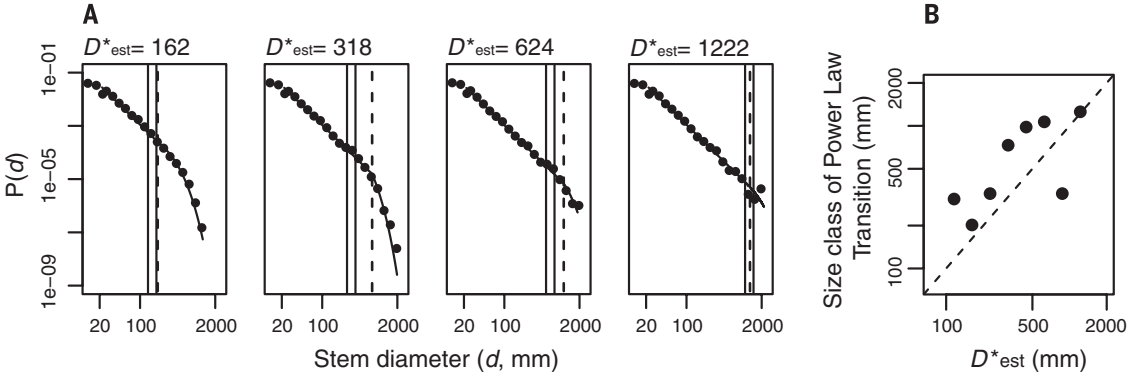

Fig. 3. Tree size distributions and forest size. (**A**) Size distributions for combined, circular, 20-m-diameter patches (points) grouped by estimated minimum diameter of canopy trees [D^*_{est} (*18*); solid vertical lines mark the range]. The power-law best fit to all data (Fig. 1) with the size class best fit for transition (dashed vertical lines) to an exponential tail is shown in black. (**B**) The full range of D^*_{est} and the size class of transition from power-law to exponential distribution.

a constant mortality rate (μ_u) the size distribution of understory trees at time t is (note: $d_c = G_c t$)

$$N_u(d,t) = \begin{cases} 0, t < \dfrac{d}{G_c} \\ \left(\dfrac{P\theta}{\phi d^{\theta+1}} - \dfrac{\mu_c}{G_c}\dfrac{P}{\phi d^{\theta}}\right) e^{-\mu_u\left(t-\frac{d}{G_c}\right)}, t \geq \dfrac{d}{G_c} \end{cases} \quad (4)$$

The expressions for N_c and N_u (Eqs. 1 and 4 and fig. S1) hold until the crown area lost by the mortality of canopy trees is greater than their increase from growth (until $t = \theta/\mu_c$). Assuming that the contribution of sites with $t > \theta/\mu_c$ is negligible, and a stochastic stand-clearing disturbance rate of μ, the landscape-level size distribution (for $d < G_c\theta/\mu_c$) is (*18*)

$$N(d) \approx \frac{P}{\phi d^{\theta}}\left(e^{-\mu\frac{d}{G_c}} - e^{-\mu\frac{d+1}{G_c}}\right) + \left(\frac{P\theta}{\phi d^{\theta+1}} - \frac{\mu_c}{G_c}\frac{P}{\phi d^{\theta}}\right)\frac{\mu}{\mu_u+\mu} e^{\frac{\mu_u d}{G_c}}\left(e^{-\frac{d}{G_c}(\mu_u+\mu)} - e^{-\frac{\theta}{\mu_c}(\mu_u+\mu)}\right) \quad (5)$$

Plotting Eq. 5 against the data and simulations (Fig. 4A, red) shows, despite simplifications, that the analytical model holds the mechanisms driving the power function shape of the size distribution. Here, the dominant power function is of the form $d^{-(\theta+1)}$ (in Eq. 5) (Fig. 4B), originating from the production of understory trees by overtopping (Eqs. 2 and 3).

In tropical forests, deviations from the power law occur at both tails, which are precisely the trees for which the overtopping process is not significant. Overtopping begins when the new seedlings are large enough to close the gap, and overtopping stops when crown area loss from canopy tree mortality catches up to gains from growth, setting, respectively, lower and upper limits on the power function.

Many terms of Eq. 5, including the upper diameter limit of applicability, may be important in forests that are unlike BCI, explaining the lack of power-law size structure in some temperate and dry tropical forests. For example, of the nine forests presented by Muller-Landau *et al.* (*5*, *10*), the two driest forests (Huai Kha Khaeng and Mudumalai) have the weakest power-law size structure. These two forests also lack evidence of the slow-growing overtopped trees that make up the power law in the model. In both the Huai Kha Khaeng and Mudumalai forests, growth rates remain high across the full range of diameters. Temperate forests also often lack power-law size structure (*25*–*27*). When parameterized with slow growth rates and infrequent stand-clearing disturbances, which are likely parameters for temperate forests (table S3), model simulations also produce a lack of power-law size structure (fig. S3).

The vital-rate scaling with size that drives the consistent power-law size structure of tropical forest trees is the scaling of the number of individuals by diameter that are experiencing the shift from fast growth in the sun to slow growth in the shade during the process of recovery from a gap disturbance (Eq. 2). In both the model and the data, the power-law size structure emerges after gap-generating disturbances (Fig. 2), and the overtopped (understory) individuals are those that follow the power law (Fig. 3). The scaling exponent of the underlying power law is dependent on only the allometric exponent of the crown area–to–diameter relationship (θ). Site-level average values of θ are consistent across diverse tropical forests (table S2), explaining the consistency of scaling of the power function.

Here, we have presented evidence that the consistency among tropical forest tree size distributions is driven by the unifying mechanisms of gap-generating disturbances and subsequent asymmetric competition for light. This explanation is in stark contrast to the energy equivalence prediction of metabolic scaling theory (*4*, *7*, *8*, *14*) and models based on demographic equilibrium (*5*, *10*, *12*, *13*), in which vital rates are constant with respect to tree size. Specifically, in order to mechanistically predict ecosystem services, including carbon storage, tropical forest models must incorporate canopy gaps [as in the Ecosystem Demography model (*28*)], the phototropic growth of individuals [as in the Perfect Plasticity Approximation model (*29*)], and the strong dependence of individual growth rates on light.

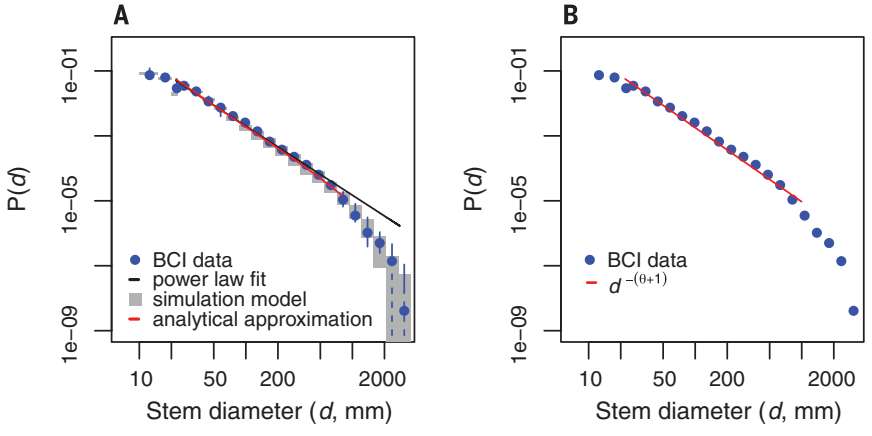

Fig. 4. Model and data comparison of tree size distributions. BCI forest dynamics plot data are shown in blue. (**A**) Data error is the 95% confidence interval for each size class from the plot cut into four subplots of 12.5 ha each (N = 28 patches). Gray boxes are simulation model results marking 95% confidence intervals for each size class (12.5 ha, N = 100 patches). The red curve shows the analytical approximation of the simulation model (Eq. 5). (**B**) BCI data (blue) compared with the dominant power-law scaling of the model ($\propto d^{-(\theta+1)}$ in Eq. 5, red).

REFERENCES AND NOTES

1. S. P. Hubbell, R. B. Foster, *Oikos* **63**, 48–61 (1992).
2. J. Q. Chambers *et al.*, *Proc. Natl. Acad. Sci. U.S.A.* **110**, 3949–3954 (2013).
3. D. C. Marvin *et al.*, *Proc. Natl. Acad. Sci. U.S.A.* **111**, E5224–E5232 (2014).
4. B. J. Enquist, K. J. Niklas, *Nature* **410**, 655–660 (2001).
5. H. C. Muller-Landau *et al.*, *Ecol. Lett.* **9**, 589–602 (2006).
6. M. P. H. Stumpf, M. A. Porter, *Science* **335**, 665–666 (2012).
7. B. J. Enquist, J. H. Brown, G. B. West, *Nature* **395**, 163–165 (1998).
8. G. B. West, J. H. Brown, B. J. Enquist, *Nature* **400**, 664–667 (1999).
9. H. Cyr, S. C. Walker, *Ecology* **85**, 1802–1804 (2004).
10. H. C. Muller-Landau *et al.*, *Ecol. Lett.* **9**, 575–588 (2006).
11. D. A. Coomes, R. B. Allen, *J. Ecol.* **95**, 1084–1097 (2007).
12. N. Rüger, R. Condit, *Funct. Ecol.* **26**, 759–765 (2012).
13. J. Lai *et al.*, *Oikos* **122**, 1636–1642 (2013).
14. B. J. Enquist, G. B. West, J. H. Brown, *Proc. Natl. Acad. Sci. U.S.A.* **106**, 7046–7051 (2009).
15. R. Condit, *Tropical Forest Census Plots* (Springer-Verlag, Berlin, Germany, and R. G. Landes Company, Georgetown, TX, 1998).
16. S. P. Hubbell *et al.*, *Science* **283**, 554–557 (1999).
17. S. P. Hubbell, R. Condit, R. B. Foster, http://ctfs.arnarb.harvard.edu/webatlas/datasets/bci (2005).
18. Materials and methods are available as supplementary materials on *Science* Online.
19. A. Clauset, C. R. Shalizi, M. E. J. Newman, *SIAM Rev.* **51**, 661–703 (2009).
20. K. Shinozaki, K. Yoda, K. Hozumi, T. Kira, *Jpn. J. Ecol.* **14**, 133–139 (1964).
21. G. B. West, B. J. Enquist, J. H. Brown, *Proc. Natl. Acad. Sci. U.S.A.* **106**, 7040–7045 (2009).
22. S. Bohlman, S. Pacala, *J. Ecol.* **100**, 508–518 (2012).
23. C. Uhl, K. Clark, N. Dezzeo, P. Maquirino, *Ecology* **69**, 751–763 (1988).
24. C. D. Canham, *Ecology* **69**, 786–795 (1988).
25. D. A. Coomes, R. P. Duncan, R. B. Allen, J. Truscott, *Ecol. Lett.* **6**, 980–989 (2003).
26. X. Wang *et al.*, *Oikos* **118**, 25–36 (2009).
27. L. I. Duncanson, R. O. Dubayah, B. J. Enquist, *Glob. Ecol. Biogeogr.* **24**, 1465–1475 (2015).
28. D. Medvigy, S. C. Wofsy, J. W. Munger, D. Y. Hollinger, P. R. Moorcroft, *J. Geophys. Res.* **114**, G01002 (2009).
29. D. W. Purves, J. W. Lichstein, N. Strigul, S. W. Pacala, *Proc. Natl. Acad. Sci. U.S.A.* **105**, 17018–17022 (2008).

ACKNOWLEDGMENTS

We thank J. Chave, H. C. Muller-Landau, and R. Chisholm for helpful discussion and L. Comita for sharing data. We gratefully acknowledge the support of the Carbon Mitigation Initiative of Princeton University and the National Institute for Mathematical and Biological Synthesis (NSF grant no. DBI-1300426, The University of Tennessee, Knoxville). The BCI forest dynamics research project was founded by S. P. Hubbell and R. B. Foster and is now managed by R. Condit, S. Lao, and R. Perez under the Center for Tropical Forest Science and Smithsonian Tropical Research in Panama. Numerous organizations have provided funding, principally in the United States. NSF and hundreds of field workers have contributed. The data are publicly available at http://ctfs.arnarb.harvard.edu/webatlas/datasets/bci.

SUPPLEMENTARY MATERIALS

www.sciencemag.org/content/351/6269/155/suppl/DC1
Materials and Methods
Supplementary Text
Figs. S1 to S3
Tables S1 to S3
Simulation Code
References (*30*–*38*)

20 August 2015; accepted 17 November 2015
10.1126/science.aad0592